Detecting Shape of Weld Defect Image on X-ray Film by Image Processing Applied Genetic Algorithm*

Kimiya AOKI** and Yasuo SUGA***

Several types of non-destructive testing methods are used for detecting weld defects. Because the X-ray radiographic testing method is particularly useful in inspecting the inside of a weld metal, it is often used in industry. However, since the number of skilled inspectors for X-ray radiographic testing has been gradually decreasing, recently, several methods to detect weld defects from films automatically have been investigated to improve the quality of the detection results. However, X-ray film images contain much noise, and defect images show very low contrast and various shapes in spite of the same kind of defect. Moreover, boundaries between a defect image and the background are unclear, making it difficult to automate the inspection of X-ray films. If the type of defect image were to be judged by an expert system or a neural network which learns the rules of professional inspectors, the boundaries of the defect image would have to be detected in a manner similar to recognition by a human's (or an inspector's) sense of vision. Therefore, in this study, a new image processing method applied genetic algorithms that were a method of optimization, was constructed and applied to the detection of defect boundaries in detail.

Key Words: Welding, Image Processing, Nondestructive Inspection, Weld Defects, X-ray Film, Genetic Algorithm

1. Introduction

Detecting weld defect images on X-ray inspection films taken from a steel welding part is a difficult image-processing problem, because X-ray films contain much particulate noise and show low contrast, defect images show various shapes in spite of the same kind of defect, and boundaries between the defect image and the background are unclear, among others. We proposed the "background subtraction method" for detecting an unclear defect image clearly[1]. In this method, brightness distribution corresponding to a welding reinforcement is initially determined as the background image, and then the defect image is detected by subtracting the background image from the original image. This method enables the determination of the existence, location, and shape of defect images in X-ray film images. Moreover, in the case of a fully automated inspection system, judgment of the type of detected defect image must be automated. For the judgment of defect type, methods that employ a neural network and an expert system have been proposed[2]-[5]. In those methods, knowledge based on defect information: location, brightness, shape and so on, which expert inspectors use at the time of judgment, is summarized as the rule.

In the case of an automatic inspection system for X-ray films by image processing, first of all, the system must recognize the existence, location and shape of a defect image. Accordingly, various methods including the background subtraction method have been proposed[1]-[9]. However, the expert system or the neural network learning the rule of professional

* Received 10th July, 2001. Japanese original: Trans. Jpn. Soc. Mech. Eng., Vol. 66, No. 644, C (2000), pp. 1380-1387 (Received 19th April, 1999)

** Department of Information and Computer Sciences, Toyohashi University of Technology, 1-1 Hibarigaoka, Tempaku-cho, Toyohashi, Aichi 441-8580, Japan (Formerly, Graduate School of Keio University)

*** Faculty of Science and Technology, Department of Mechanical Engineering, Keio University, 3-14-1 Hiyoshi, Kouhoku-ku, Yokohama, Kanagawa 223-8522, Japan. E-mail: suga@mech.keio.ac.jp

inspectors during visual inspection is utilized for judging the type of detected defect image, in which case the detailed shape of the defect image is detected. That is to say, in order to improve the type judgment rate, it is necessary to detect the unclear boundary of the defect image in a manner similar to recognition by a human's sense of vision. Therefore, in this study, we focused on detecting the shape of weld defect images in a domain where the existence of defect was expected by pre-processing. First, we pointed out that comparatively uncertain processing based on the human's pattern recognition system enabled visual detection of defect boundaries. Then, we considered the human's visual and proposed top-down image processing. Concretely, in the proposal method, many patterns having various shapes are superimposed on an original X-ray image, and the most suitable one is chosen as the defect shape. In order to perform this search process efficiently, the genetic algorithm (GA) was applied for pattern generation and selection.

2. X-ray Images Taken from Steel Welding Part and Experimental Setup

The relationship between weld beads and X-ray films is shown in Fig. 1. X-ray inspection is one of the known non-destructive inspection methods. Recording the X-ray dosage transmitted through a weld part on a film shows the inside of the weld metal. By X-ray inspection, the reinforcement is taken as a white area, and if a defect exists in a weld bead, it appears on the bead image as a shadow (local low-brightness area) according to its size, shape, density and type. X-ray films used in this study are acquired by X-ray inspection of welded joints of steel pipes obtained by the submerged-arc welding process. These film images are digitized and processed by the image processing system shown in Fig. 2. The image scanner, which has a lighting unit for transparent film, and a personal computer make up the film inspection system. According to the general size of weld defects, the resolution of image data is 480 *dpi* and the gray scale is 256 *levels* (8 bit). Therefore, the spatial resolution is approximately 0.053 *mm* per pixel.

3. Characteristic of Defect Images

3.1 Characteristic of X-ray film images

Figure 3 shows an original image including a blowhole and its brightness distribution. X-ray films have low contrast, contain much particulate noise and have an uneven background in general. Defect images are mixed with the brightness distribution corresponding to reinforcement. These factors make detection of defect images difficult. Also, defect images have various shapes, sizes and degrees of brightness in spite

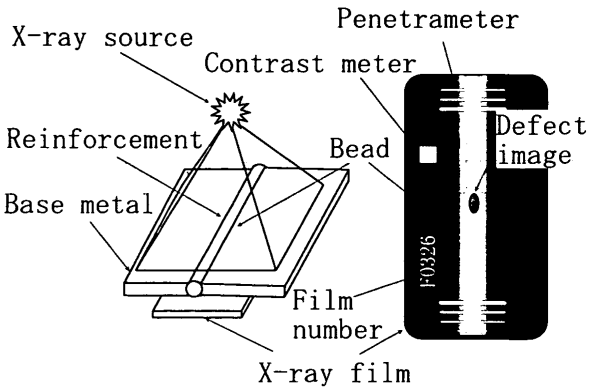

(a) X-ray inspection (b) Result

Fig. 1 Relationship between weld bead and X-ray film

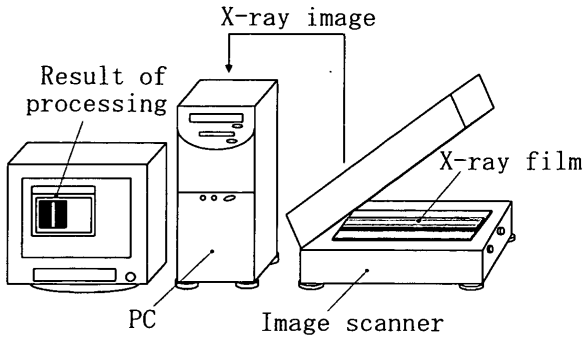

Fig. 2 Arrangement of equipment

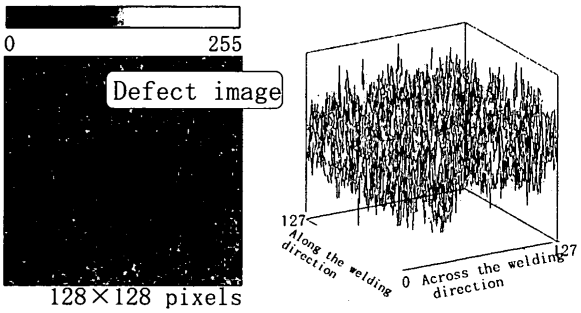

(a) Original image (b) Brigtness distribution

Fig. 3 Characteristic of X-ray film image

of the same kind of defect. Moreover, the boundary between defect images and the background focused in this study is extremely unclear. Thus, these factors may lead to differences in shape between defect images detected by automatic image processing and that by a professional inspector's visual test.

3.2 Conditions for detection of defect boundaries by visual sense

Figure 4 shows binary images obtained by binarization of original images. From Fig. 4(b), it is confirmed that the detection of defect images is difficult by only simple binarization because of the

uneven brightness distribution due to reinforcement. The main point is that boundaries are detected with particles. Moreover, when the defect image shows low contrast globally as shown in Fig. 4(c), the whole image is detected as a set of particles. Then, the threshold for binarization is gradually changed, and a defect image is observed. Figure 5 shows an example of this experiment. When the threshold is set at 165, the defect image appears as a high-density region of white particles. As the boundary, the threshold that facilitates pattern recognition differs according to the local section of the boundary.

From Fig. 5, it is shown that X-ray film images contain much particulate noise and defect images are also composed of lower brightness particles (pixels). The density and brightness of particles seem to affect the detection of the boundary on each local section. In a visual test by inspectors, a smooth boundary line seems to be drawn, separating the defect area from the background according to the density and brightness of particles, and the defect pattern is recognized.

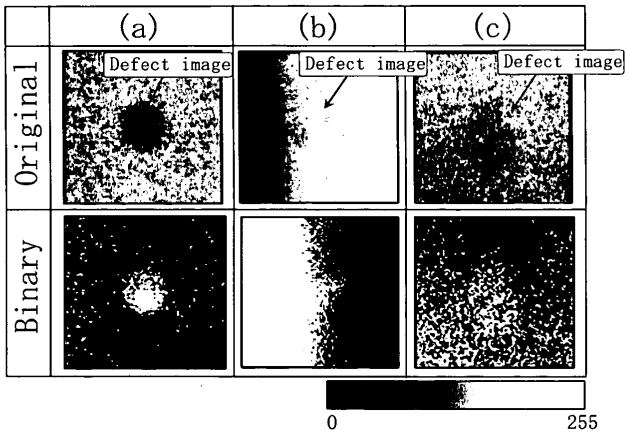

Fig. 4 Characteristic of defect image

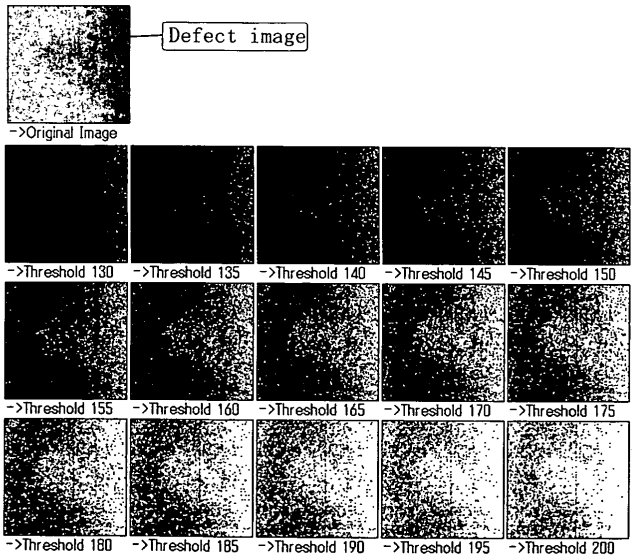

Fig. 5 Characteristic of defect image

As mentioned above, the distribution and the brightness of particles (pixels) in film images provide information for the detection of defect images. Therefore, if a local image processing method such as spatial filtering, or morphological operation is applied, the detection result may be different from the visual impression because particle information is destroyed. Accordingly, in this study, image processing not by the bottom-up method in which defect images are detected as a result of combining local processing of each pixel, but by the top-down method was adopted. That is to say, many patterns prepared beforehand are superimposed on an original image including a defect image one by one, and the most well-fit pattern as the defect image is chosen. This is the top-down method.

4. Applying GA to Image Processing for Defect Shape Detection

4.1 Outline of processing

The basic idea of the proposed algorithm is that many patterns having various shapes are superimposed on an original image, and the most well-fit one is chosen as the defect shape. The detection of a smooth boundary line in particles becomes possible by fitting patterns. However, the shapes defect images may take vary and the fitting process is difficult. In order to realize search processing, genetic algorithm (GA)[10], which has been used in computer science as one of the optimization methods, was applied. In applying GA, the important tasks are as follows: the method for cording phenotype (a defect image pattern) to genotype is defined; the evaluation rule for fitness between a pattern with an arbitrary shape and a defect image is defined; a detection system using GA operation is constructed in order to realize good search.

In this study, the processing window is set on a bead image containing a defect, as shown in Fig. 6. The size of the window is 128^2 pixels square. The base point C is set at the center of the processing window. The defect image may be a closed region including the base point C. The searching process of the boundary line consists of the three main steps. In the first step, a defect area is detected roughly using elliptical patterns. In the second step, the defect image is detected as a polygonal pattern in the elliptical pattern detected at the first step. In the third step, concaves and convexes of the polygonal pattern detected at the second step are adjusted delicately at many points on the sides in order to detect the defect boundary with higher resolution. Different methods of coding and fitness calculations are defined for each step, and

effective search is realized. The processing and definitions are described below.

4.2 Definition of fitness

It is important that an evaluation rule for the matching rate between a pattern with an arbitrary shape and a defect image be defined, as shown in Fig. 7. This rate is "*fitness*" in GA operation. Two fitness calculation rules based on the conditions for the recognition of a defect image (as mentioned in section 3) were proposed.

First of all, the base value of contrast S_{base} in the processing window is calculated. Brightness values belonging to the processing window are sorted. Then, the average values of brightness belonging 1/4 of higher rank and lower rank respectively are calculated, and their difference is defined as S_{base}.

4.2.1 ***Fitness 1*** Figure 7(b) shows the area setting for the calculation of fitness of particles comprising the whole area of the pattern. The inside area of the fitted pattern is defined as area A, and the surrounding area is set around area A by means of dilation processing at d times and defined as area B. The value d is adjusted so that area A and area B become approximately equal. If the fitted pattern is similar to a defect shape in the processing window, the lower brightness particles in area A will have a bigger influence on the recognition of the defect image than the higher one. Therefore, the local minimum filter $(m \times m)$ is applied to area A, and the local median filter is applied to area B for decreasing noise as background. Then, the average brightness values are calculated in both areas, and difference between these average values is divided by S_{base} and defined as fitness. At this time, to decrease global brightness unevenness on the background, the area of the pattern is divided into four parts, as shown in Fig. 7(b) and fitness is calculated for each part. Finally, the four fitness values are averaged and that is *fitness 1*. The higher *fitness 1* is, the higher the contrast of the fitted pattern is, and the closer to a defect image it is. The calculation rule of *fitness 1* is summarized as follows.

if $((\bar{B}_{f\text{-}med} - \bar{A}_{f\text{-}min}) > 0)$

$$fitness\ 1 = (\bar{B}_{f\text{-}med} - \bar{A}_{f\text{-}min})/S_{base}$$

else

$$fitness\ 1 = 0.000\,000 \qquad (1)$$

Figure 8 shows the validity of *fitness 1*. First, the defect image in the original image (a) is detected by visual method on a display (Fig. 8(b)). Dilation and erosion processing are applied to the detected defect pattern and the generated patterns are labeled 'E5 ~D5'. An experiment is conducted compare *fitness 1*

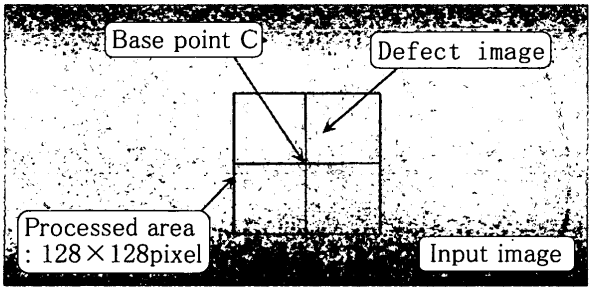

Fig. 6 Previous processing

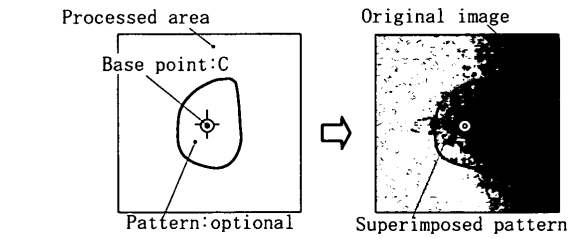

(a) Principle of evaluation

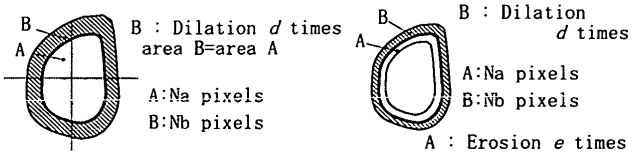

(b) Fitness 1 (c) Fitness 2

Fig. 7 Definition of fitness

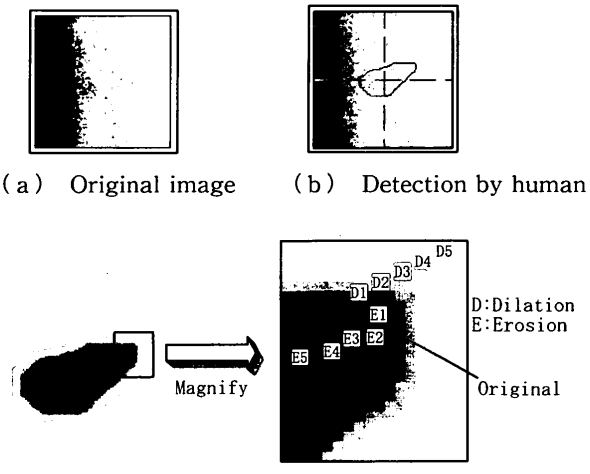

(a) Original image (b) Detection by human

(c) Definition of sample

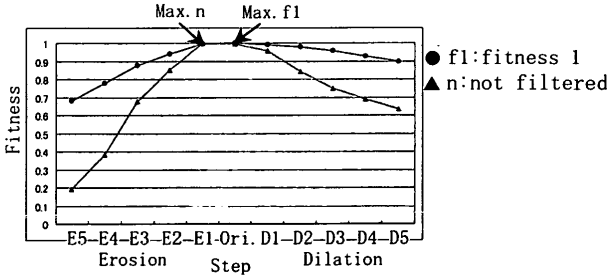

(d) Fitness

Fig. 8 Effect of fitness 1

calculated by Eq.(1) with the simple matching rate (contrast between area A and area B) calculated without the filtering process on each labeled pattern. The result of this experiment is shown in Fig. 8(d). In every case (E5~D5), *fitness 1* is higher than the simple matching rate. In particular, because of the effect of local filtering, the fitness value increases if the fitted pattern does not match slightly, so the search progresses smoothly. Using the proposal *fitness 1*, even if the contrast of defect images is very low, it is possible that defect shapes close to visual inspection are detected.

4.2.2 ***Fitness 2*** Figure 7(c) shows the area setting for calculation of fitness of particles comprising the adjacent areas of a boundary line. The outside and inside areas are set on both sides of the fitted pattern by dilation (d times) and erosion (e times) processing. The inside area is indicated by A and the outside area, by B. The local minimum filter ($m \times m$) is applied to area A, and *fitness 2* is calculated in the same manner as *fitness 1*. The calculation rule of *fitness 2* is summarized as follows.

if $((\bar{B}-\bar{A}_{f\text{-}\min})>0)$

$fitness\ 2=(\bar{B}-A_{f\text{-}\min})/S_{base}$

else

$fitness\ 2=0.000\,000$ (2)

Fitness 2 responds only to particle distribution at the area adjacent to the boundary line and can evaluate the pattern's outline more precisely than *fitness 1*. However, because a search result may get trapped into local solution in the case of irrelevant application, it is necessary to limit the search area to the area adjacent to the boundary line.

It is possible to adjust change sensitivity of fitness to a pattern shape using filter size m. Thus, the adjustment of m with the progress of search steps enables calculation of adequate values as fitness.

4.3 Coding pattern

A method that codes phenotype to genotype is important in GA. In this study, because the search object is a candidate for a defect shape, the phenotype is a binary pattern expressing a defect image. The coding methods for each search step are explained below.

4.3.1 Focusing search area by elliptical pattern (*GP1*) Figure 9 shows the relationship between phenotype and genotype at the first search step. A defect area is detected roughly using elliptical patterns and the search area in later steps is limited. From Fig. 9(a), the elliptical pattern used in searching has five parameters: coordinates [(r_{cent} ; [$0 \leqq r_{cent} \leqq R_c$]), ($\theta_{cent}$; [$0 \leqq \theta_{cent} \leqq 2\pi$])] of the center point C', lengths of the major and minor axes (a, b) ; [ab-min $\leqq (a, b) \leqq ab$-max], and rotation angle θ_{rot} ; [$0 \leqq \theta_{rot} \leqq$

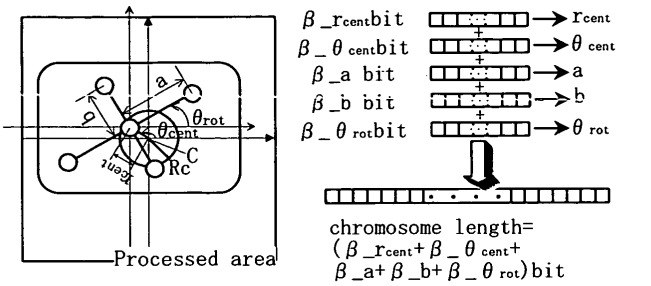

(a) Definition of genotype

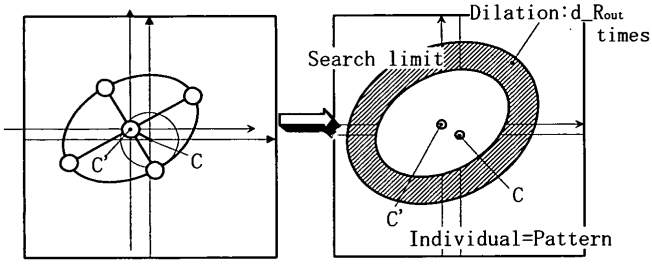

(b) Definition of phenotype

Fig. 9 Genotype and Phenotype 1 (GP1)

π]. These parameters are converted into binary numbers and combined. This bit line is defined as a chromosome. The bit length for each parameter is β-r_{cent}, β-θ_{cent}, β-a, β-b, and β-θ_{rot} bit, respectively. In decoding, each section in the chromosome corresponding to each of the parameters is converted into a decimal number and normalized with parameter ranges. This operation is given by the equations below. In these equations, $(\ )_2$ indicates binary number and $(\ )_{10}$, decimal number.

$(r_{cent}\ ;\ \beta\text{-}r_{cent})_2 \rightarrow (r'_{cent})_{10}$

$$r_{cent}=(r'_{cent}/(2^{\beta\text{-}r_{cent}}-1))\cdot R_c \quad (3)$$

$(\theta_{cent}\ ;\ \beta\text{-}\theta_{cent})_2 \rightarrow (\theta'_{cent})_{10}$

$$\theta_{cent}=(\theta'_{cent}/(2^{\beta\text{-}\theta_{cent}}-1))\cdot 2\pi \quad (4)$$

$(a\ ;\ \beta\text{-}a)_2 \rightarrow (a')_{10}$

$$a=ab\text{-}\min+(a'/(2^{\beta\text{-}a}-1))\cdot(ab\text{-}\max-ab\text{-}\min) \quad (5)$$

$(b\ ;\ \beta\text{-}b)_2 \rightarrow (b')_{10}$

$$b=ab\text{-}\min+(b'/(2^{\beta\text{-}b}-1))\cdot(ab\text{-}\max-ab\text{-}\min) \quad (6)$$

$(\theta_{rot}\ ;\ \beta\text{-}\theta_{rot}) \rightarrow (\theta'_{rot})_{10}$

$$\theta_{rot}=(\theta'_{rot}/(2^{\beta\text{-}\theta_{rot}}-1))\cdot\pi \quad (7)$$

The elliptical pattern searches the processing window for the defect region by changing its center point, major and minor axes and rotation angle. Finally, dilation processing is applied d-R_{out} times to the elliptical pattern chosen as the candidate for the defect region and this pattern is defined as the limited search area in the second step.

4.3.2 Rough search by polygonal patterns (*GP2*) Figure 10 shows the relationship between

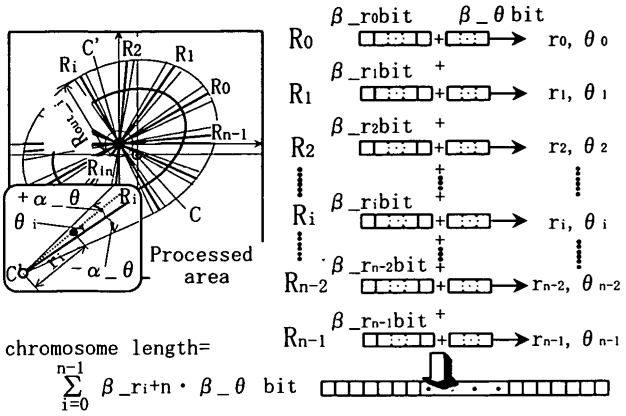

(a) Definition of genotype

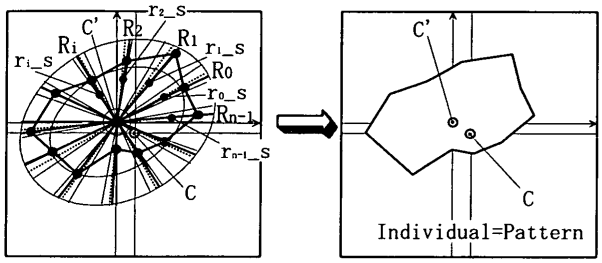

(b) Definition of phenotype

Fig. 10 Genotype and Phenotype 2 (GP2)

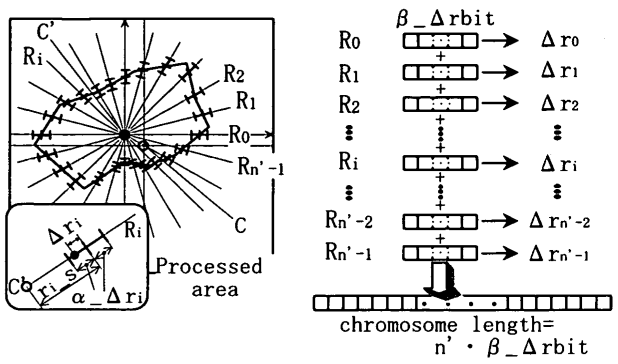

(a) Definition of genotype

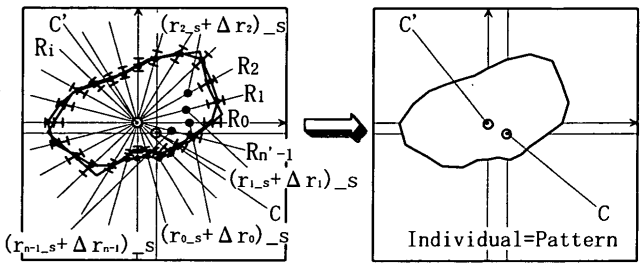

(b) Definition of phenotype

Fig. 11 Genotype and Phenotype 3 (GP3)

phenotype and genotype in the second search step. A defect shape is detected roughly using polygonal patterns with n apexes. First, from Fig. 10(a), tentacles R_i (baselines) radiating from the center point C' are set. Apexes belonging to the polygonal pattern are set on each tentacle. The section that the apex n_i is set on, is limited to $[R_{in} \sim R_{outi}]$. The apexes have two parameters: $(r_i, \theta_i).r_i$; $[R_{in} \leqq r_i \leqq R_{outi}]$ is R_i direction length and θ_i; $[-\alpha\_\theta \leqq \theta_i \leqq +\alpha\_\theta]$ is swing angle from the initial position. These parameters are converted into binary numbers and the bit lengths for the two parameters are β_r_i, and β_θ bit, respectively. These bit lines are combined and defined as the chromosome corresponding to apex n_i. It is noted that the search limitation R_{outi} differs for each apex n_i, because the search area is limited by the ellipse. Therefore, bit length β_r_i is adjusted adequately for each tentacle. The chromosome for arbitrary polygonal patterns is constructed by combining n bit lines for apexes. The above operation is given by below equations and the decoding process is the same as that of *GP1*.

$$(r_i\,;\ \beta\_r_i)_2 \rightarrow (r_i')_{10}$$

$$r_i = R_{in} + (r_i'/(2^{\beta\_r_i}-1)) \cdot (R_{out_i} - R_{in}) \qquad (8)$$

$$(\theta_i\,;\ \beta\_\theta)_2 \rightarrow (\theta_i')_{10}$$

$$\theta_i = ((\theta_i'/(2^{\beta\_\theta}-1)) \cdot 2\alpha\_\theta) - \alpha\_\theta \qquad (9)$$

Lines connect apexes and the polygonal pattern is constructed. At that time, smoothing is applied in order to eliminate an extremely acute angle, as shown in Fig. 10(b). In calculating the new coordinate of the apex, the apex adjacent to it has a bigger influence by parameter γ. The smoothed r_i is given below by equations as r_i_s.

$$r_i\_s = (\gamma\_1 \cdot r_{i-1} + \gamma \cdot r_i + \gamma\_2 \cdot r_{i+1}) / (\gamma + \gamma\_1 + \gamma\_2)$$

$$\gamma\_1 = (0.5/\alpha\_\theta) \cdot \theta_{i-1} + 1.0$$

$$\gamma\_2 = -(0.5/\alpha\_\theta) \cdot \theta_{i+1} + 1.0 \qquad (10)$$

4.3.3 Detection of defect shape in detail (*GP3*) Figure 11 shows the relationship between phenotype and genotype in the third search step. A defect shape is detected in detail by changing the polygonal pattern obtained in the second search step. That is to say, concaves and convexes of the polygonal pattern detected by *GP2* are adjusted delicately at many points on its sides in order to detect the defect boundary with higher resolution. First, from Fig. 11(a), n' tentacles R_i radiating from the center point C' are set, and then the length r_i_s between the point where the tentacle crosses the pattern outline and point C' is determined. The polygonal pattern shape is adjusted slightly by adding Δr_i; $[-\alpha\_\Delta r_i \leqq \Delta r_i \leqq +\alpha\_\Delta r_i]$ to r_i_s. This Δr_i is converted into binary numbers whose length is $\beta\_\Delta r_i$ bit, and the chromosome for the degree of regulation is constructed by combining n' bit lines. The range of regulation $\alpha\_\Delta r_i$ is set at approximately ten percent of r_i_s. Δr_i is given by the equations below.

$(\Delta r_i\ ;\ \beta\_\Delta r)_2 \rightarrow (\Delta r_i')_{10}$

$$\Delta r_i = ((\Delta r_i'/(2^{\beta\_\Delta r}-1)) \cdot 2\alpha\_\Delta r_i) - \alpha\_\Delta r_i \qquad (11)$$

The number of tentacles increases or decreases with the length of the adjusted outline, that is, the length of the chromosome also changes. When the apexes are connected and adjusted, the polygonal pattern is constructed, and smoothing is also applied. Smoothed $(r_{i\_s}+\Delta r_i)$ is given by the equation below.

$$(r_{i\_s}+\Delta r_i)_{\_s} = ((r_{i-1\_s}+\Delta r_{i-1}) + \gamma(r_{i\_s}+\Delta r_i) + (r_{i+1\_s}+\Delta r_{i+1}))/(\gamma+2) \qquad (12)$$

4.4 Rule of selection, crossover and mutation[10]

4.4.1 Selection The number of individuals being searched is P. In generation, individuals are arranged according to fitness values, and those in the lower rank $[(1-s\_rate)\times 100\%]$ are eliminated. Then, a couple is chosen from the higher rank at random, and a new individual is reproduced by crossover operation. The number of individuals is constant. Using this selection method, a reasonable solution is realized within a short time.

4.4.2 Crossover and mutation Uniform crossover is adopted for crossover operation in this study. In uniform crossover, bit values of children chromosomes are succeeded on each locus from parents A and B with succession rates $[c\_rate\ ;\ A, (1-c\_rate)\ ;\ B]$, respectively, and so the locus having a different bit value between parents A and B in the children chromosome is only adjusted at random in proportion as a crop of individuals converges. Therefore, because each section in the chromosome corresponds to apex's coordinates of a polygonal pattern generated by the proposed definition of coding (*GP2* and *GP3*), it may be expected that patterns having various shapes are generated in the early generation and the outline is adjusted delicately with progress of generation.

Concerning mutation operation, the bit value is turned over 0 to 1 or 1 to 0 on each locus by the mutation rate $[m\_rate]$, which decreases gradually on searching.

4.5 Processing flow

Figure 12 shows the entire processing flowchart. As mentioned above, the process of searching for a boundary line consists of three main stages. In the first stage, a defect area is detected roughly by *GP1*; the defect image is approximated by a polygonal pattern by *GP2* in the second stage; and finally, the defect shape is detected by *GP3* in the third stage. First of all, the processing window and the base point C are set in the input X-ray film image.

The common GA operation unit is used in all stages. First, P individuals are generated at random with bit lines as chromosomes. Then, each individual's chromosome is decoded to the pattern as the phenotype and given fitness values, and the individuals are arranged according to their fitness values. Moreover, selection, crossover and mutation operation are carried out in sequence, and the individuals are evaluated by the fitness. This unit of search processing is performed by the initial number of maximum generation G on each stage.

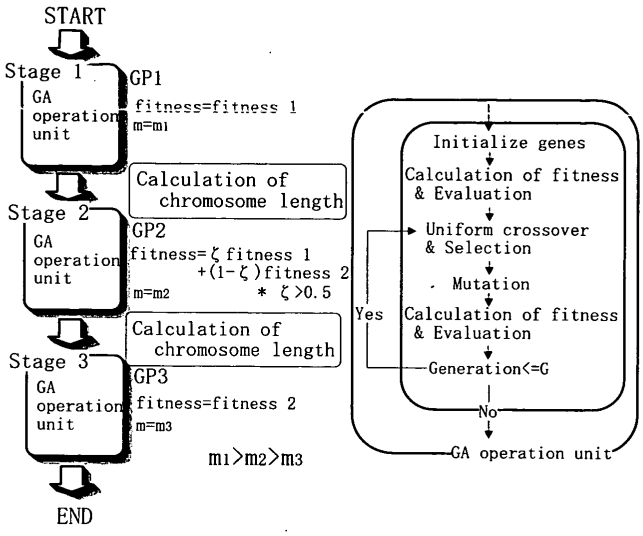

(a) Flowchart (b) GA operation unit

Fig. 12 Flowchart of image processing using GA

Because the first stage is roughly searched by *GP1* to focus on the search area, *fitness 1* is used for evaluation of individuals (elliptical patterns). In the second stage, *GP2* is applied to the individual with the highest fitness value given in the first stage, and is used for calculating the fitness value combining *fitness 1* and *fitness 2*. In the third stage, *GP3* is applied to the individual with the highest fitness value given in the second stage, and only *fitness 2* is used because in this stage, search is limited to the neighborhood of a defect boundary.

5. Effect of *GP* Change

If a higher search accuracy is required, it is necessary to increase the resolution of a polygonal pattern by increasing the number of tentacles and digitization of the tentacles. However, increasing the resolution means increasing the length of a chromosome and an explosive expansion of the number of search patterns, because the search area is not focused in the early stage. In this study, gradual processing from global search to local search and from rough search to detailed search is realized without increasing the length of the chromosome by means of *GP* change on search. Detection resolution finally becomes higher. After the first stage (*GP2* and *GP3*), the chromosome length changes according to the pattern sent from the former stage; thus, search time is shorted in the case of a small defect. Moreover,

Table 1 Search conditions

(a)Fitness

Size of processed area S=128×128pixels	
fitness 1	fitness 2
Dilation d areaB>=areaA	Dilation d=3times Erosion e=3times
Size of filter m1=7pixel m2=5pixel m3=3pixel	

(b)First stage

Genotype and Phenotype GP1	GA operation
Bit length β_r_{cent}=3bit β_θ_{cent}=6bit β_a=4bit β_b=4bit β_θ_{rot}=6bit chromosome length=23bit Search limits r_{cent};0～10pixel θ_{cent};0～2π a, b;15～45pixel θ_{rot};0～π Dilation d_Rout=10times	Population P=50 Selection s_rate=0.4 Crossover c_rate=0.5 Mutation m_rate=0.05～0.00 Max. generation G=30

(C)Second stage

Genotype and Phenotype GP2	GA operation
Feeler Ri n=12 Bit length β_r_i=1～4bit β_θ=2bit chromosome length=36～72bit Search limits r_i;5～55pixel θ_i;-5～+5° Smoothing weight γ=2or3	Population P=50 Selection s_rate=0.4 Crossover c_rate=0.5 Mutation m_rate=0.05～0.00 Max. generation G=50 Fitness weight ζ=0.8

(d)Third stage

Genotype and Phenotype GP3	GA operation
Feeler Ri n=12～24 Bit length $\beta\_\Delta r$=2bit chromosome length=24～48bit Search limits Δr_i;r_{i_s}×0.2pixel Smoothing weight γ=2	Population P=50 Selection s_rate=0.4 Crossover c_rate=0.5 Mutation m_rate=0.05～0.00 Max. generation G=50

according to the search stage, *fitness 1*, which can evaluate more globally, and *fitness 2*, which is used in local evaluation, are combined, and the local filter size m is reduced in order to obtain an adequate fitness value for the search resolution.

6. Estimation of Algorithms

The proposed algorithm mentioned above was applied to 25 film images obtained by actual X-ray inspection. The search conditions are shown in Table 1. Detection of defect shape was successful in about 23 of the 25 film images. Figure 13 shows examples of detection results. Although it was difficult that the defect image including compatibly high brightness cluster of particles was detected with shape close to visual impression, good results were obtained for other defect images in Fig. 13.

It is possible to generate 23 bit, 72 bit and 48 bit patterns in the first, second and third stages, respectively, under these search conditions (Table 1), and detection can be completed by searching of less than about 4000 patterns in total. As mentioned above, it is confirmed that the proposed image processing applying GA can effectively detect the outline of a defect in X-ray images.

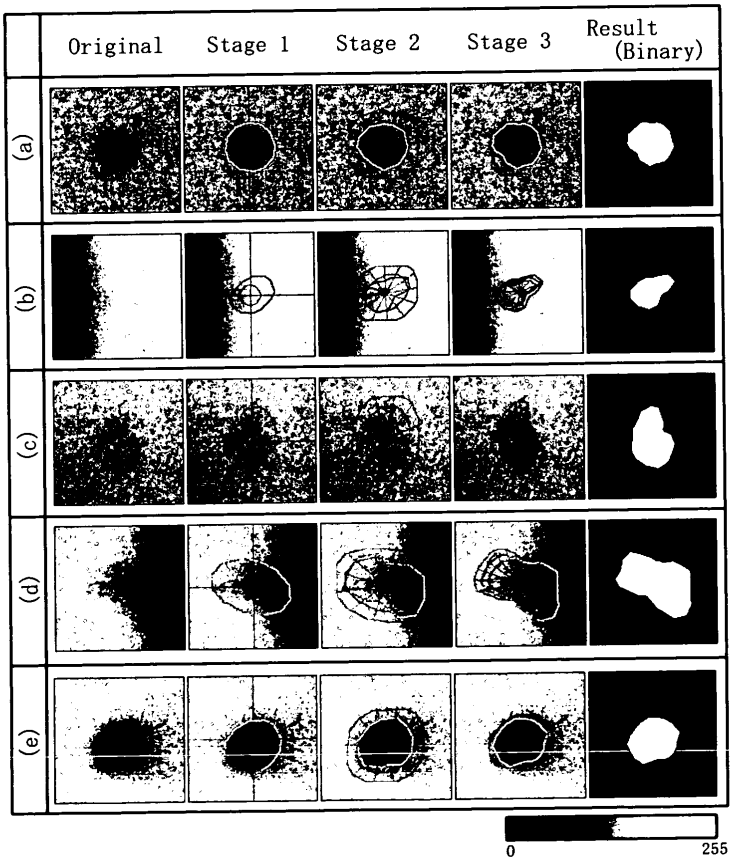

Fig. 13 Effect of processing

7. Conclusion

In this study, we proposed an image processing method applying GA, which enabled detection of a defect in X-ray images with close to visual inspection, and showed its effectiveness by experiment. The main results are summarized as follows:

(1) It was shown that defect images in X-ray films were composed of local lower brightness particles. The distribution and brightness of particles in the film image provide information for the detection of the boundary between the defect image and the background.

(2) As a method of detecting defect image, GA in which the most well-fit pattern is selected from many arbitrary patterns by evaluation of particle distribution was proposed. It makes detection of a defect boundary close to that by visual inspection possible.

(3) Two methods for the evaluation of matching rate (*fitness*) between an arbitrary pattern and a defect image were proposed. In these fitness calculation methods, in order to evaluate the density and brightness of particles adequately, different types of local filters are applied inside and outside the pattern, respectively.

(4) Methods for coding an arbitrary pattern to a bit line were proposed. Gradual processing from global search to local search and from rough search to detailed search was realized without increasing the length of the chromosome by *GP* change on search.

(5) An experiment on the detection of a defect from actual X-ray inspection film was performed, and the validity of the proposed algorithms was shown.

If the type of defect that was obtained by the proposed image processing were judged by means of a conventional system for discriminating the type of defect, an improvement of recognition rate would be expected. Then, the performance of the automatic film inspection system would be improved.

References

(1) Aoki Kimiya, Yoshida Yuuki and Suga Yasuo, Abstraction of Unclear Weld Defect Images from X-ray Film by Background Subtraction Method and Region Growing Method, Trans. Jpn. Soc. Mech. Eng., (in Japanese), Vol. 65, No. 634, C (1999), pp. 2561-2567.

(2) Koshimizu Hiroyasu, An Analytical Investigation on the Utilization of Knowledges of Experts by Using the Software System for Welding Inspections, Technical Report of the Institute of Electronics, Information and Communication Engineers, (in Japanese), PRL Vol. 84, No. 60 (1984), pp. 61-72.

(3) Aoki Kimiya, Suga Yasuo, Tominaga Teturo and Higo Masashi, On the Recognition of Weld Defects in an X-ray Inspection Film by Image Processing, Proc. of the 1st Symposium on Sensing via Image Information, (in Japanese), (1995), pp. 177-182.

(4) Kawano Seishiro, Automatic Inspection System for Radiographic Testing Using Image Processing and Artificial Intelligence Technique, Journal of the Japanese Society for Non-destructive Inspection, (in Japanese), Vol. 45, No. 8 (1996), pp. 578-585.

(5) Tanaka Haruhisa, Higo Masashi, Aoki Kimiya and Suga Yasuo, Proc. of the 2nd Symposium on Sensing via Image Information, (in Japanese), (1996), pp. 283-288.

(6) Itoga Kouyou, Sugimoto Kouji, Mitiba Kouji, Kato Yuuhei, Sugita Yuuji and Onnda Katuhiro, Welding Technique, (in Japanese), No. 9 (1990), pp. 102-107.

(7) Aoki Akio and Unishi Hiroyuki, Digital Image Processing Applied to Radiographs (1), Journal of the Japanese Society for Non-destructive Inspection, (in Japanese), Vo. 33, No. 2 (1983), pp. 108-109.

(8) Ishii Akira, Lachkhia Vakhtang, Ochi Yasuo and Akutsu Masayuki, Recognition of Internal Weld Defects by Defect Model, Trans. Jpn. Soc. Mech. Eng., (in Japanese), Vol. 60, No. 578, A (1994), pp. 2440-2445.

(9) Sato Shinya, Shibukawa Katsuhisa, Kishinami Takeshi and Ishii Akira, Automatic Detection of Internal Weld Defects on X-ray Radiographic Films, Journal of the Japan Society for Precision Engineering, (in Japanese), Vol. 64, No. 4 (1998), pp. 573-577.

(10) Agui Takeshi and Nagao Tomoharu, Genetic Algorithm, (in Japanese), (1993), pp. 53-107, Shokodo.